

Investigating Frequency Contents of Capnogram using Fast Fourier Transform (FFT) and Autoregressive Modeling (AR)

Mohsen Kazemi, M.B. Malarvili

Faculty of Biosciences and Medical Engineering, Universiti Teknologi Malaysia, 81310 Johor, Malaysia
mohsenkazemi@biomedical.utm.my

Abstract: In this paper, frequency contents of capnogram signals are investigated. Capnogram is the graphical output of capnograph and it is able to show different changes in expiratory. Capnography is the monitoring of the CO₂ level during respiration. This method is not only non-invasive, easy to do, and relatively inexpensive, but also in recent years medical societies, representing anaesthesiology, cardiology, critical care, paediatrics, respiratory care, and emergency medicine, have mandated or recommended it. Hence, processing this signal will help understanding the nature of capnogram to use for diagnosis variety of respiratory disorders. In this study, fast Fourier transform (FFT), and autoregressive (AR) modelling-Burg Method have been used to calculate power spectral density (PSD) in normal capnogram and asthmatic ones to compare the results possibility of using this analysis for diagnosis and prognosis purpose. The preliminary results show that, frequency properties of capnogram signal significantly can be used to distinguished asthmatic and non-asthmatic patients. In conclusion, these results reveal the potential of using these characteristic of capnogram signal to differentiate a variety of breathing difficulties that will help medical practitioners involved in respiratory care.

[Mohsen Kazemi, M.B. Malarvili. **Investigating Frequency Contents of Capnogram using Fast Fourier Transform (FFT) and Autoregressive Modeling (AR)**. *Life Sci J* 2017;14(10):71-78]. ISSN: 1097-8135 (Print) / ISSN: 2372-613X (Online). <http://www.lifesciencesite.com>. 11. doi:[10.7537/marslsj141017.11](https://doi.org/10.7537/marslsj141017.11).

Keywords: Autoregressive modeling; Burg Method; Capnogram; Fast Fourier transform; Windowing

1. Introduction

The history of capnograph and capnogram goes back to time physiologists recognized early on that continuous analysis of CO₂ is important to the measurement and understanding of intrapulmonary gas mixing and ventilation/perfusion relationships. The importance of continuous analysis of CO₂ has been further enhanced by simultaneous analysis of gas volumes [1].

Capnography is based on the fact that CO₂ molecules absorb infrared radiation (IR) at a specific wavelength and the amount of light absorbed is directly proportional to the concentration of the CO₂ molecules [2]. This amount of light absorbed by CO₂, which is then calculated and displayed as a numerical value or a waveform on the capnograph as a function of either time or expired volume that this waveform is known as capnogram. In other words, capnogram is the graphical display of instantaneous CO₂ concentration (mmHg) versus time (second) and is able to show the different respiratory situation of patients.

One of the Capnography benefits in field care is confirmation of bronchospasm (or obstruction in the breathing circuit). Other use of capnography is to monitor patient ventilation, and provides an early warning system of impending respiratory crisis that can be divided in two categories: hyperventilation and hypoventilation [3]. Figure 1 (a) shows a normal capnogram in comparison with an asthmatic

capnogram in figure 2 (b). It should be considered that the ascending limb of the capnogram is prolonged and is not flat, as it should be normally.

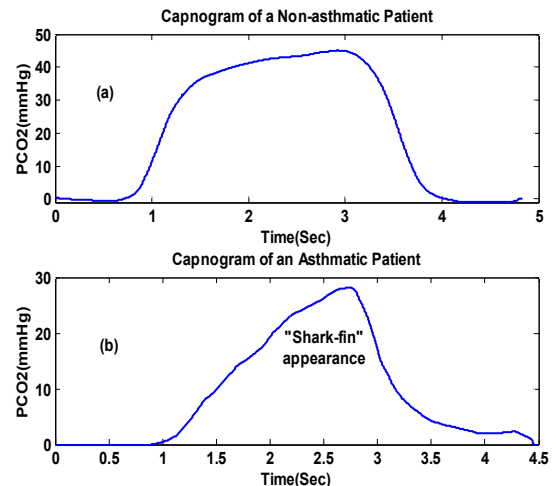


Figure 1: (a) A normal capnogram in comparison with an asthmatic one

These variations in capnogram of different diseases cause the researchers carry out analysis of this signal to differentiate between a range of illnesses that may affect this signal [4]-[8]. However, all these previous studies are conducted through time domain techniques and based on assumption that capnogram is a stationary signal. But, according to the new

findings, capnogram is a wide-sense nonstationary signal that means time-varying information is useful [9].

Accordingly, in this study, frequency properties of capnogram signal are investigated and compared in two different states; non-asthmatic and asthmatic patients. For this mean, fast Fourier transform (FFT), and autoregressive modeling (AR) are used to apply on capnogram signals, and their results are compared. Therefore, in this paper, section 2 discusses the methods that consist of data acquisition, preprocessing, FFT analysis, AR modeling of capnogram signals, and performance measure. It is continued with results and discussion at section 3. Lastly, the conclusion is presented in section 4.

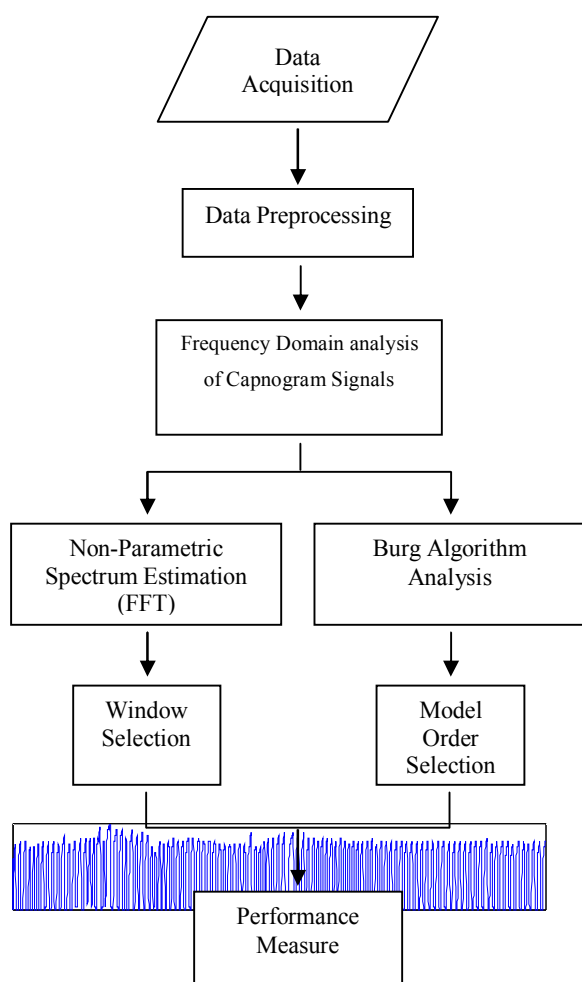


Figure 2: The overall algorithm of used method

2. Methods

Figure 2 shows overall algorithm of this section. As shown in this figure, in this section, 5 sub-steps are presented. The first step is data collection, followed by the preprocessing of capnogram signals. Then, the

frequency contents of capnogram for both normal and asthmatic ones are investigated using FFT and AR modeling in subsections 2.3 and 2.4. Lastly, in subsection 2.5, the effectiveness of the capnogram frequency property is validated by using receiver operating characteristic (ROC) curve analysis. This is to evaluate the potential of these properties to differentiate asthmatic and non-asthmatic patients (and probably other respiratory difficulties) in future.

2.1. Data Acquisition

The capnogram data were collected from patients with complaints of asthma and breathing difficulties at the Emergency Department of Hospital Pulau Pinang. Informed written consent was obtained from the patients under permission of National Medical Research Section of Ministry of Health Malaysia (MOH) that was approved by the ethics committee of Hospital Pulau Pinang. It should be noted that ethics committee of Hospital Pulau Pinang has approved this study.

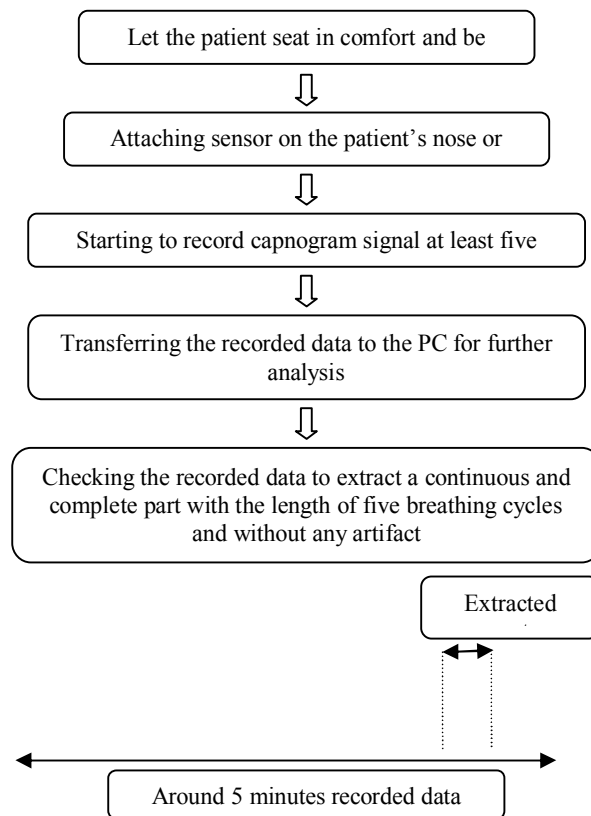


Figure 3: The block diagram for data collection

As the first step to collect data, the capnography sensor was attached on the mouth or nose of the patients. Mainstream capnography method was used in the process of data collection because this method has higher accuracy [10]. After attaching the sensor on the patient's nose or mouth, the continuous

capnogram was recorded using the capnography patient monitor, Capnostream™20 Model CS08798. Then, the capnogram data was transferred to a personal computer for analysis. Throughout the study, a total of 23 non-asthmatic capnogram, and 73 asthmatic capnogram were successfully collected. The capnogram for each patient was recorded around five minutes at a sampling frequency of 200Hz. Then, a continuous and complete part of recorded data with the length of five breathing cycles and without any artefact (approximately 20 seconds; according to the patient's respiratory rate) was extracted for further analysis. Figure 3 shows the block diagram of data collection in brief.

In our database, each sample has an ID which is used in this paper. This ID consists of 3 alphabet letters and a number. The alphabet letter is either CAP (Capnogram of Asthmatic Patient) or CNP (Capnogram of Non-asthmatic Patient) and a number right after the letters which indicates the sample number, e.g. CAP2 means the second asthmatic sample and CNP6 means the sixth non-asthmatic sample.

2.2. Preprocessing

Data preprocessing was carried out to eliminate unnecessary noise in the recorded capnogram signals. In this paper, the moving average filtering method was used to smooth the curve due to its simplicity and efficiency, especially for eliminating the high frequency noises within the signals [11]. This method smoothes data by replacing each data point with the average of neighboring data points defined within a specific span. This process is equivalent to lowpass filtering with the response of the smoothing given by the difference equation as follow:

$$y(n) = (y(n+M) + y(n+M-1) + \dots + y(n-M)) / (2M+1) \quad (1)$$

where $y(n)$ is the smoothed value for the n^{th} data point, M is the number of neighboring data points on either side of $y(n)$, and $2M+1$ is the span. Indeed, the *span* defines a window that moves across the data set as the smoothed response value is calculated for each predictor value. A large span increases the smoothness but decreases the resolution of the smoothed data set, while a small span decreases the smoothness but increases the resolution of the smoothed data set [12]. The optimal span value depends on the data set and usually requires some trial and error to determine [13]. In this study, we used the span as 13, because it produced the best results for both smoothness and resolution. Furthermore, the correlation coefficients calculated for each signal after filtering justified this span width.

2.3. FFT Analysis (Non-Parametric Spectrum Estimation)

The discrete Fourier transform (DFT) of an N -point sequence $x(n)$ is defined as:

$$X(k) = \sum_{n=0}^{N-1} x(n) e^{-j2\pi nk/N} \quad (2)$$

Because $x(n)$ may be either real or complex, evaluating $X(k)$ requires on the order of N complex multiplications and N complex additions for each value of k . Therefore, because there are N values of $X(k)$, computing an N -point DFT requires N^2 complex multiplications and additions. The fast Fourier transform (FFT) is a fast algorithm to compute the DFT which involves decomposing an N -point DFT into successively smaller DFTs [14].

One of the major applications of the FFT is in analyzing the frequency content of continuous-time signals. In many cases of practical interest, these waveforms are neither periodic nor aperiodic, but a segment of a much longer, and possibly infinite, time series, e.g. EEG, and ECG. Obviously, only a portion of such waveforms can be represented in the finite memory of the computer, and some attention must be paid to how the waveform is truncated, i.e. the need for multiplication of discrete-time signal $x(n)$ by a window $w(n)$, as a consequence of the finite-length requirement of the FFT.

2.3.1. Window Selection

Some commonly used windows are Rectangular, Bartlett (triangular), Hanning, Hamming, and Blackman, and all of them have the property that

$$w(n) = \begin{cases} w(M-n) & 0 \leq n \leq M \\ 0 & \text{Otherwise} \end{cases} \quad (3)$$

i.e., they are symmetric about the point $M/2$, and as a result their Fourier transforms are of the form

$$W(e^{j\omega}) = W_e(e^{j\omega}) e^{-j\omega M/2} \quad (4)$$

The bottom line is that, when a data set is windowed, the frequency characteristics of the window become part of the spectral results. In this regard, all windows produce some artefacts that could be obtained by taking the Fourier transform of the window itself. In general, all windows produce two types of artefacts. It means that, the actual spectrum is widened by an artefact termed the main-lobe, and additional peaks are generated termed side-lobes. Moreover, reduced resolution, and leakage are two primary effects on the spectrum as a result of applying window to the signal, that the resolution is influenced primarily by the width of the main-lobe of $W(e^{j\omega})$, while the degree of leakage depends on the relative amplitude of the main-lobe and the side-lobes of $W(e^{j\omega})$ [15]. Table 1 is a comparison of commonly used windows [16].

The fourth column of Table 1 shows the peak approximation error in decibels (dB) for the windows. Clearly, the windows with the smaller side-lobes yield better approximations of the ideal response at a discontinuity. Also, the third column, which shows the

width of the main-lobe, suggests that narrower transition regions can be achieved by increasing M . But the bottom line about window length is that, a wide window gives better frequency resolution but

poor time resolution and a narrower window gives good time resolution but poor frequency resolution [16].

Table 1: Comparison of commonly used windows (M is window length)

| Type of Window | Peak Side-Lobe (Relative) | Amplitude Approximate Main-Lobe | Width of Peak Approximation Error, $20 \log_{10} \delta$ (dB) |
|----------------|---------------------------|---------------------------------|---|
| Rectangular | -13 | $4\pi/(M+1)$ | -21 |
| Bartlett | -25 | $8\pi/M$ | -25 |
| Hanning | -31 | $8\pi/M$ | -44 |
| Hamming | -41 | $8\pi/M$ | -53 |
| Blackman | -57 | $12\pi/M$ | -74 |

In our process, Blackman window with $M=256$ is selected since the capnogram is biomedical signal related to the respiratory system. So, they are in the category of low frequency signals [17], and selecting this number as length of window does not affect the time-resolution.

A Blackman window is in the form of:

$$w(n) = \begin{cases} 0.42 - 0.5 \cos(2\pi n/M) + 0.08 \cos(4\pi n/M) \\ 0 \end{cases} \quad (5)$$

One of the advantages of the Blackman window according to Table 1 is that it greatly reduced the side-lobes besides a high side-lobe roll-off rate, although the main-lobe's bandwidth has increased, however the extra width is usually worth the trade-off [16].

It should be considered that to avoid confusing side-lobe peaks with main-lobe ones, the definition of $\Omega_M = 2\pi/M$ (M is window length) is used. In principle, each side-lobe has width Ω_M , as measured between zero crossings, and the main-lobe, on the other hand, must be at least $2\Omega_M$ wide too to be considered real [18].

2.4. AR Modeling (Parametric Spectrum Estimation)

A variety of AR models are currently used to estimate the power spectral density (PSD) of biomedical signals. The Burg method was selected because, as shown in Eq. 8 and 9, it estimates the reflection coefficients, but other methods such as autocorrelation approach, use prediction coefficients for the AR process. So, in comparison with other approaches such as autocorrelation, covariance, modified covariance, and recursive least squares (RLS), this method does not require run-off of the data sequence by zero padding and has minimal phase characteristic with high accuracy, and stability [19].

Autoregressive (AR) models are widely used for power spectral density (PSD) estimation [20]. The AR model of a time series is represented in the following form:

$$X(n) = - \sum_{m=1}^P a(m) X(n-m) + e(n) \quad (6)$$

where $X(n)$ is the time series, $a(m)$ are AR parameters, p is the model order, and $e(n)$ is the prediction error. The minimization criteria of the Burg method are obtained by minimizing the sum-squared of the forward and backward prediction errors as follows:

$$E \triangleq \sum_{n=p}^{N-1} [e_p^f(n)^2 + e_p^b(n)^2] = \min \quad (7)$$

where $e_p^f(n)$ is the forward prediction error at the p th stage, $e_p^b(n)$ is the backward prediction error at the p th stage, N is the total number of data points, and P represents the model order. Burg minimized the performance index with respect to the reflection coefficients as follows:

$$\frac{\partial E}{\partial \gamma_p} = 2 \sum_{n=p}^{N-1} \left[e_p^f(n) \frac{\partial e_p^f(n)}{\partial \gamma_p} + e_p^b(n) \frac{\partial e_p^b(n)}{\partial \gamma_p} \right] = 0 \quad (8)$$

where γ_p are the reflection coefficients. Then, the forward and backward prediction errors can be calculated by using lattice filters and as a result, the reflection coefficients γ_p can be obtained as follows:

$$\gamma_p = \frac{2 \sum_{n=p}^{N-1} e_{p-1}^f(n) e_{p-1}^b(n-1)}{\sum_{n=p}^{N-1} [e_{p-1}^f(n)^2 + e_{p-1}^b(n-1)^2]} \quad (9)$$

Consequently, the power spectrum can be estimated as:

$$P_{XX}^{BUR}(\omega) = \frac{\sigma_e^2}{|1 + \sum_{k=1}^P a(k) e^{-j\omega k \Delta n}|^2} \quad (10)$$

where σ_e^2 is the constant noise power, ω is the frequency, and Δn represents the sampling interval, and P is model order.

One of the crucial parts for the Burg algorithm analysis is the selection appropriate value for the model order P . In spectral estimation, the accuracy of the estimated spectrum is critically dependent on the model order that is chosen. It means that a too low model order can generate an over smoothed spectrum, whereas too high a value of order may introduce

spurious details such as false peaks into spectrum [21].

The model order can be estimated using the Akaike information criterion (AIC) which is one of the most popular approaches to determine an optimum model order and minimize the information entropy of the signal identified as follows [21]:

$$AIC(P) = N \ln(E_p) + 2P \quad (11)$$

where E_p , P , and N individually represent the estimation of mean-squared error, the order of the filter, and the number of input signal samples.

In this study, the AIC for different model orders were calculated. As shown by the results in figure 4, at $P=10$ the AIC value was smallest compared to the other number of P . So, the model order 10 was selected since the minimum of error variance was observed at this value of P .

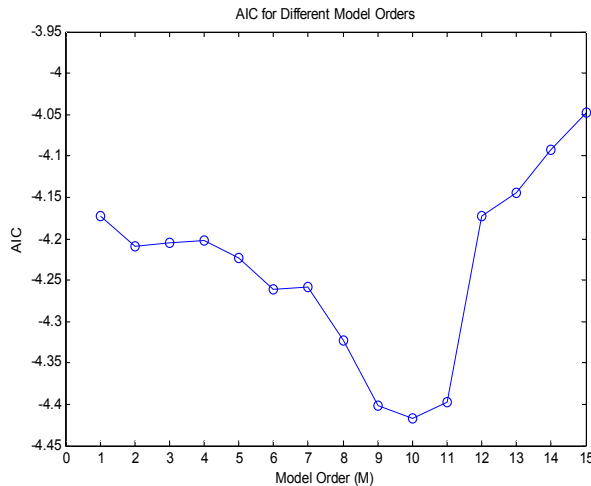


Figure 4: AIC values for different model orders

2.5. Performance Measure

The effectiveness of extracted features is assessed by Receiver Operating Characteristic (ROC) curve analysis and two indices included sensitivity and specificity that are often employed in medical applications [22]. The results of a particular test are considered in two categories; in our case, asthmatic and non-asthmatic patients. There will be some cases with the disease correctly classified as positive (TP = True Positive fraction), and some cases with the disease will be classified negative (FN = False Negative fraction). On the other hand, some cases without the disease will be correctly classified as negative (TN = True Negative fraction), but some cases without the disease will be classified as positive (FP = False Positive fraction). According to this classification, sensitivity and specificity that estimate the classifier's performance in different classes [23], define as follow:

$$Sensitivity = TP / (TP + FN)$$

$$Specificity = TN / (TN + FP)$$

So, *Sensitivity* is probability that the capnogram test result will be positive when the disease is present, and *Specificity* is probability that the capnogram test result will be negative when the disease is not present.

Furthermore, with ROC curves, when the variable under study cannot distinguish between the two groups, the area under the ROC curve (AUC) will be same to 0.5, whereas when there is a perfect separation of the values of the two groups, the AUC becomes 1. Also the P-value is the probability that the sample AUC is found when the true category area under the ROC curve is 0.5 (null hypothesis: Area = 0.5). If P is low ($P < 0.05$) then it can be concluded that the area under the ROC curve is significantly different from 0.5 and that therefore there is evidence that the capnogram test does have an ability to distinguish between the two groups [24].

3. Results and Discussion

In this section, the results of FFT analysis, and the estimated PSD using AR modeling-Burg method are thoroughly presented and discussed.

3.1. FFT Analysis Results

After selecting the appropriate window, the FFT analysis was applied on the capnograms of asthmatic and non-asthmatic patients. Figure 5 and figure 6 show the FFT of the capnogram of a non-asthmatic patient (CNP2) and the capnogram of an asthmatic patient (CAP9), respectively. It should be noted that to estimate spectrum of capnogram signals, DC value has been removed, so the first peak is not happen at zero frequency.

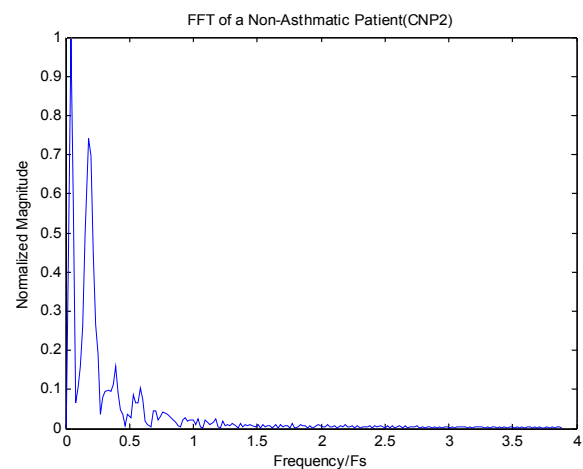


Figure 5: The FFT of a non-asthmatic capnogram (CNP2)

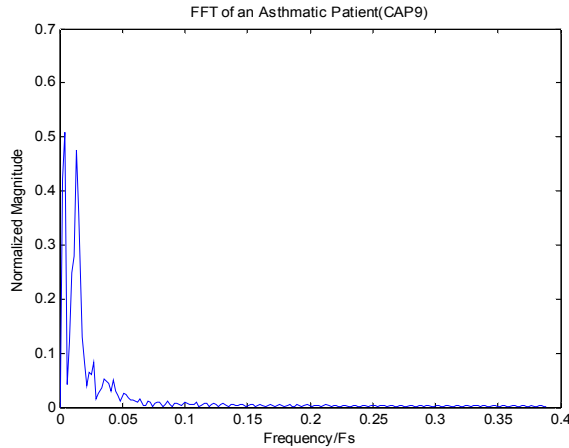


Figure 6: The FFT of an asthmatic capnogram (CAP9)

Based on figure 5 and figure 6 and the results for all data, there was a significant difference between the number of component and their magnitudes in the spectrum of CAPs and CNPs. With reference to the definition of Ω_M in method, section 2.3.1, the number of main-lobe in the asthmatic capnogram was equal to 2 in contrast to non-asthmatic capnogram, which had only 1 main-lobe. Also, the frequency of these components and their related bandwidth were also different in both asthmatic and non-asthmatic samples. For asthmatic patient, the normalized frequency and bandwidth of the first component were around 0.078 and 0.23, respectively, whereas for non-

asthmatic patients these values for only component were around 0.04 and 0.08, respectively.

Moreover, the normalized magnitude of the first component in both asthmatic and non-asthmatic capnogram had significant difference, i.e. the average of normalized magnitude of the first component in non-asthmatic capnogram was around 0.85, in comparison with the average of normalized magnitude of the first component in asthmatic capnogram that was around 0.43.

Table 2 shows the performance indices of the magnitude, frequency, and bandwidth of the dominant peak in the spectrum of CNPs, and CAPs. For this mean, power spectrum of all CNPs and CAPs have been estimated using spectrum, and then performance indices have been extracted for the magnitude, frequency, and bandwidth of the main-lobe in spectrum of all capnogram signals.

Based on the Table 2, all features have AUC > 0.8 and p-value < 0.0001. This shows that all features of the dominant peak in the spectrum of CAPs and CNPs are possible to be applied in the differentiation of the asthmatic conditions. However, compared to all the features, it can be seen that the bandwidth of the main-lobe and its magnitude have noticeable AUC (with p-value < 0.0001), sensitivity (96.77 and 97.54, respectively) and specificity (94.74 and 94.63, respectively) which is considerably more efficient to classify the capnogram data, and to differentiate the asthmatic conditions.

Table 2: Performance indices of the magnitude, frequency, and bandwidth of the main-lobe in the FFT of CNPs, and CAPs

| <i>Performance index</i> | <i>Magnitude of the main-lobe (Normalized)</i> | <i>Frequency of the main-lobe (Hz)</i> | <i>Bandwidth of the main-lobe (Hz)</i> |
|--------------------------|--|--|--|
| Sensitivity | 97.54 | 80.65 | 96.77 |
| Specificity | 94.63 | 82.11 | 94.74 |
| AUC | 0.937 | 0.847 | 0.975 |
| P-Value | <0.0001 | <0.0001 | <0.0001 |

3.2 Burg Algorithm Analysis Results

Figure 7 and figure 8 show the PSD estimation of a non-asthmatic capnogram (CNP2) and an asthmatic capnogram (CAP9) by using Burg method of AR modelling approach. It should be noted that to estimate spectrum of capnogram signals, DC value has been removed, so the first peak is not happen at zero frequency.

As figure 7 and figure 8 shown, and according to the results for all collected data, the PSD estimation of the non-asthmatic capnogram signals (CNPs) consists of one component, while for asthmatic capnogram signals (CAPs), this estimation produced two components. Hence by using the second component in PSD estimation using Burg method, asthmatic and non-asthmatic conditions can be differentiated

completely. In addition, the frequency of the first component, and the total power of the PSD estimation for asthmatic capnogram were around 0.02 Hz and 0.195, respectively, whereas, these values for non-asthmatic capnogram were around 0.011 Hz and 0.354, respectively. Also, the normalized magnitude of the first component in both asthmatic and non-asthmatic capnogram had significant difference, i.e. the average of this value in non-asthmatic capnogram was around 0.83, in comparison with the average of normalized magnitude of the first component in asthmatic capnogram that was around 0.37.

Table 3 shows performance indices for the frequency of the first component, its magnitude, and the total power in the PSD estimation of the CAPs and CNPs via Burg method. For this mean, power

spectrum of all CNPs and CAPs have been estimated using Burg algorithm, and then performance indices have been extracted for the frequency of the first component, its magnitude, and the total power in the PSD estimation of all CNPs, and CAPs.

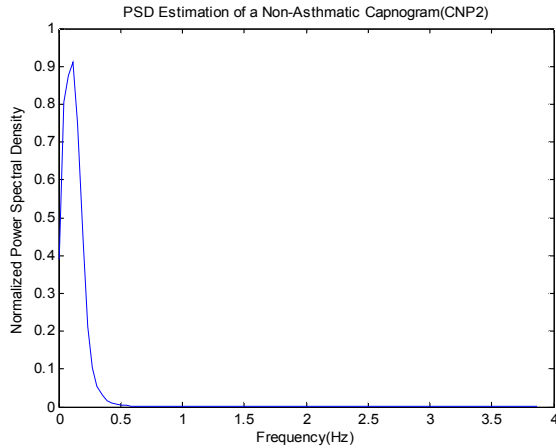


Figure 7: Power spectral density of a non-asthmatic capnogram (CNP2)

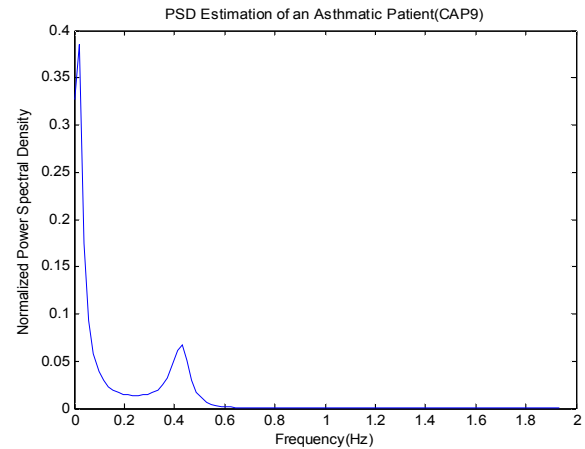


Figure 8: Power spectral density of an asthmatic capnogram (CAP9)

Table 3: Performance indices of the frequency of the first component, its magnitude, and the total power in the PSD estimation of CNPs, and CAPs

| <i>Performance index</i> | <i>Frequency of the First Component (Hz)</i> | <i>First Magnitude of the Component (Normalized)</i> | <i>First Total Power</i> |
|--------------------------|--|--|--------------------------|
| Sensitivity | 98.23 | 98.3 | 83.87 |
| Specificity | 95.08 | 93.8 | 84.21 |
| AUC | 0.996 | 0.97 | 0.722 |
| P-Value | <0.0001 | <0.0001 | 0.0023 |

According to the Table 3, all the features in the PSD estimation have AUC > 0.7 and p-value < 0.003. This indicated that all features in the PSD distribution of CAPs and CNPs were functional in differentiating the asthmatic and non-asthmatic conditions. However, it is obvious that the first component frequency and its magnitude have noticeable AUC and p-value < 0.0001, accompanied by high sensitivity and specificity, which is efficient to classify the capnogram signals in two groups. As a result, these parameters and the frequency of the second component (that only exist in PSD of asthmatic patients) can significantly differentiate the asthmatic conditions.

The fact is that, the frequency of the second component of the asthmatic capnograms PSD estimation varied in patients with different levels of asthmatic severity. It means that, the average of this value for the very low, low, mild, and serious asthmatic capnograms was around 0.18 (Hz), 0.25(Hz), 0.43(Hz), and 0.6(Hz), respectively. Therefore, this component not only can be used to

differentiate the asthmatic and non-asthmatic conditions, but also can be used as a crucial feature to classify the asthmatic capnogram signals with different levels of severity.

4. Conclusion

Capnogram is a vital representation of the respiratory system. Therefore, the analysis of this physiological signal could lead to the development of computerized methods to differentiate airway disorders, which could benefit both the healthcare professional involved in respiratory care and the patients. Previous studies conducted for capnogram signal analysis used only conventional time domain methods. In this paper, for the first time, frequency contents of capnogram signals of asthmatic and non-asthmatic patients have been investigated. The results showed that by using these properties, asthmatic and non-asthmatic conditions can be perfectly differentiated. Also, by the incorporation of a GRBF neural network in near future, the severity of asthma in the patients could be automatically assessed as a

new index in capnographs. This method is an innovative idea that could further assist the medical practitioners as it would be possible to monitor severity of asthma and other respiratory disorders automatically and instantaneously with minimum human errors.

Acknowledgements:

This work was supported by the Ministry of Higher Education Malaysia. The authors gratefully acknowledge the Universiti Teknologi Malaysia (UTM) for providing facilities and laboratory equipments. Special thanks to Dr. Aik Howe Teo from Hospital Pulau Pinang for his medical consultations and Mr. Tan Teik Kant for his assistance in data collection.

Corresponding Author:

Dr. Mohsen Kazemi

Faculty of Bioscience and Medical Engineering,
Universiti Teknologi Malaysia, 81310 Johor,
Malaysia

E-mail: mohsenkazemi@biomedical.utm.my

References

1. Steven Weinberger, E. Barbara Cockrill, A. and Jess Mandel. *Principles of pulmonary medicine*. 5th Edition. Elsevier Inc. 2008.
2. Mohsen Kazemi, Nur Ilham Imarah, M. B. Malarvili "Assessment on Methods Used to Detect Asthmatic and Non-asthmatic Conditions using Capnogram Signal", *Jurnal Teknologi (Sciences & Engineering)*, 2013, Vol. 62, No. 1, pp. 93-100, DOI: 10.11113/jt.v62.1179.
3. Teo, A. H. Kamaruddin Jaalam. Rashidi Ahmad. Chew Keng Sheng. and Nik Hisamuddin, N. A. R. The use of end-tidal capnography to monitor non-intubated patients presenting with acute exacerbation of asthma in the emergency department. *Journal of emergency Medicine*. 2009, 41(6): 581-589.
4. Krauss Baruch "Advances in the Use of Capnography for Nonintubated Patients" *Israeli Journal of Emergency Medicine*, 2008, 8(3), pp. 3-15.
5. Einav Sharon, Matot Idit "Computrized Continuous Capnography for Prediction of Survival from Resuscitation" *Journal of Resuscitation*, 2008, 77, pp. 34-40.
6. Druck J, Rubio PM, Valley MA, Jaffe MB, Yaron M (2007) Evaluation of the slope of phase III from the volumetric capnogram as a non-effort dependent in acute asthma exacerbation. *Ann. Emerg. Med.* 50(3): pp. 130-136.
7. Tan Teik Kean, Teo AH, Malarvili MB "Feature extraction of capnogram for asthmatic patient." In *Proceedings of IEEE Int. Conf. on Computer Engineering and Applications*: Malaysia, 2010, pp. 251-255.
8. Pablo V. Romero, and Lluís Blanch "Volumetric Capnography in Acute Respiratory Distress Syndrome" *Pulmao R J*, 2011, 20(1), pp. 37-41.
9. Mohsen Kazemi, Malarvili MB "Investigation of Capnogram Signal Characteristics using Statistical Methods." In *Proceedings of the IEEE-EMBS Conference on Biomedical Engineering and Sciences (IECBES)*: Langkawi, Malaysia, 2012, pp. 343-348.
10. Julie Swenson, Piedad N Henao-Guerrero, James W Carpenter, Clinical technique: use of capnography in small mammal anesthesia, *J. Exot. Pet Med.* 17(3) (2008) 175-180.
11. Martti Kirkko-Jaakkola, Jussi Collin, Jarmo Takala, Bias prediction for MEMS gyroscopes, *IEEE Sens. J.* 12(6) (2012) 2157-2163.
12. Andrea Facchinetti, Giovanni Sparacino, Claudio Cobelli, An online self-tunable method to denoise CGM sensor data, *IEEE Trans. Biomed. Eng.* 57(3) (2010) 634-641.
13. Gonzalo R Arce, *Nonlinear Signal Processing; A Statistical Approach*, New Jersey, John Wiley & Sons, Inc., 2005.
14. Guohun Zhu, Yan Li, Peng (Paul) Wen "Epileptic seizure detection in EEGs signals using a fast weighted horizontal visibility algorithm" *Journal of Computer Methods and Programs in Biomedicine*, 2014, 115 (2), pp. 64-75.
15. John Semmlow, L. *Biosignal and Biomedical Image Processing*. Marcel Dekker Inc. 2004.
16. Alan Oppenheim, V. and Ronald Schaffer, W. *Discrete-Time Signal Processing*. 3rd Edition, Prentice Hall Signal Processing Series. 2010.
17. Lauralee Sherwood. *Fundamentals of Physiology: A Human Perspective*. Thomson Brooks and Cole Inc. 2006.
18. Julius Smith, O. *Spectral Audio Signal Processing*. Stanford University: W3K Publishing. 2011.
19. Blinowska, K. J. and Zygierevicz, J. *Practical Biomedical Signal Analysis*. Poland: CRC Press (Taylor & Francis Group, LLC). 2011.
20. Han-Wen Hsu. and Chi-Min Liu. Autoregressive Modeling of Temporal/Spectral Envelopes with Finite-Length Discrete Trigonometric Transforms. *IEEE Transactions on Signal Processing*. 2010, 58(7): 3692-3705.
21. Tracey Cassar. Kenneth Camilleri, P. Simon Fabri, G. Order Estimation of Multivariate ARMA Models. *IEEE journal of Selected Topics in Signal Processing*. 2010, 4(3): 494-503.
22. Andriy Temko, Gordon Lightbody, Eoin M Thomas, Geraldine B Boyland, William Marnane, Instantaneous measure of EEG channel importance for improved patient-adaptive neonatal seizure detection, *IEEE Trans. Biomed. Engineering* 59(3) (2012) 717-727.
23. M.M. Fraz, P. Remagnino, A. Hoppe, B. Uyyanonvara, A.R. Rudnicka, C.G. Owen, S.A. Barman "Blood vessel segmentation methodologies in retinal images – A survey" *Journal of Computer Methods and Programs in Biomedicine*, 2012, 108(1), pp. 407-433.
24. Hanan Mostafa Kamel, Abdel-Halim El-Sayed Amin and Ahmed Reda El-Adawy. Endothelial and Some Cytokine Inflammatory Markers as Risk Factors of Hypertension in Postmenopausal Women. *Life Sci J* 2014;11(3):220-223.

10/23/2017